J Mater Sci (2008) 43:5720–5727
DOI 10.1007/s10853-008-2890-9

Microstructure and wear assessment of TIG surface alloying of CP-titanium with silicon

F. Adib Hajbagheri · S. F. Kashani Bozorg · A. A. Amadeh

Received: 3 May 2008 / Accepted: 18 July 2008 / Published online: 13 August 2008

Abstract Tungsten Inert Gas (TIG) process has been employed to produce surface alloyed tracks on preplaced CP-Ti substrate with Si to improve wear resistance. Uniform alloyed tracks with hypo eutectic binary Ti–Si compositions have been achieved using preplaced layers with Si amounts of up to 40 at.%. Si content of the TIG alloyed tracks was found to be affected by the TIG heat input and Si amount of the preplaced layer. The microstructures of the surface alloyed tracks showed phases of primary α-Ti in dendrites and eutectic lamellas of α-Ti and Ti_5Si_3 within the interdendritic regions using optical and scanning electron microscopy, X-ray diffractometry, and energy dispersive spectroscopy. Finer dendrites were found at lower heat input. A maximum micro hardness value of 750 HV was found in the surface alloyed track, which is ~4 to 5 times of that of the substrate material (180 HV). Pin-on-disk wear tests exhibited the better performance of the surface alloyed tracks than the untreated material which is attributed to the presence of Ti_5Si_3 intermetallic compound in the microstructure.

Introduction

Titanium and its alloys are extensively used in aerospace, chemical, and marine industries, owing to their specific strength, good corrosion resistance, and high temperature properties [1]. On the other hand, relatively low shear strength, high coefficient of friction, and low hardness value allow titanium to be damaged by adhesive wear mechanisms [2, 3]. Inadequate wear resistance imposes a limitation on titanium and its alloys for a wider range of applications. Resistance to wear is a surface phenomenon and is mainly determined by the material's surface properties rather than its bulk properties. Surface modification is one of the most efficient means to improve the tribological properties of titanium alloys. In the last decades, several surface modification techniques have been employed to improve the wear properties of titanium and its alloys, including physical and chemical vapor deposition [4], [5], ion implantation [6], pack cementation [7], electron [8, 9], and laser [10, 11] beam surface processing. Physical deposition techniques are associated with relatively long fabrication time and thin surface layers, while techniques such as electron and laser beam use a highly concentrated heat which can melt a surface layer and produce relatively thick processed layer on the substrate materials.

Surface modification using a concentrated heating source such as laser or electron beam radiation permits the chemical composition and microstructure of a relatively thicker surface layer of a material to be tailored to withstand wear resistance under high loading condition. Dutta Majumdar et al. used laser beam for surface modification of Ti alloy with Si addition and reported improved surface properties [12, 13]. However, electron and laser beam surface processing techniques are limited by several factors, such as need for vacuum chamber, costly manufacturing procedure, and expensive initial investments [5–10].

Recently, a novel process for surface modification was developed using a Tungsten Inert Gas (TIG) torch [14, 15]. In the process of TIG surface melting, a torch with adequate

F. A. Hajbagheri · S. F. Kashani Bozorg (✉) · A. A. Amadeh
School of Metallurgy and Materials Engineering, University College of Engineering, University of Tehran,
P.O. Box 11155-4563, Tehran, Iran
e-mail: fkashani@ut.ac.ir

power density is passed over the surface of a substrate in which a large amount of energy is absorbed in a short time interval and results in a liquid/substrate interface which moves toward the substrate and within a fraction of a second, a molten pool region inside the substrate forms; due to the existence of temperature gradients across the surface layer and the underlying substrate, the TIG melt pool is rapidly solidified to form a layer with metallurgical bond to the substrate material. Short processing time; flexibility in operation; economy in time, energy, and material consumption; and processing precision are the important advantages of TIG surface alloying process. Limited works are reported on the applications of this process for surface modification of titanium alloys [16, 17].

In the present study, TIG surface alloying of a preplaced CP-Ti substrate with silicon powder was carried out under an atmosphere of pure argon gas. The microstructure of the surface alloyed tracks is characterized using optical and scanning electron microscopy and X-ray diffractometry. Also, wear assessment of the TIG alloyed layers are presented.

Experimental procedure

Commercial pure (CP) titanium was used as a substrate in the form of 100 mm × 60 mm sheet with a thickness of 5 mm. The substrates were cleaned with an ultrasonic cleaner prior to surface processing, and then washed thoroughly with alcohol to remove any dust particles and maintain the specific condition.

Titanium and silicon powders were mixed in a ball mill with different percentages of Si powder according to Table 1. Few drops of sodium silicate, as a binder, was mixed with the powder mixture and then placed on the substrate surface to form even layers with the thickness of ~1.2 mm. The binder helps the powder not to be blown during glazing action. Also, it can protect the melt from oxidation upon cooling from high temperature. Prior to the TIG process, the preplaced substrate was dried in an oven. An x–y positioning table was used which could be moved by a hydraulic machine. The speed of the table could be

Table 1 TIG surface alloying parameters

Track no.	Si in preplaced layer (at.%)	Current (A)	Substrate traverse speed (mm/min)
1	20	125	200
2	30	125	200
3	30	80	200
4	30	90	100
5	40	125	200
6	50	125	200

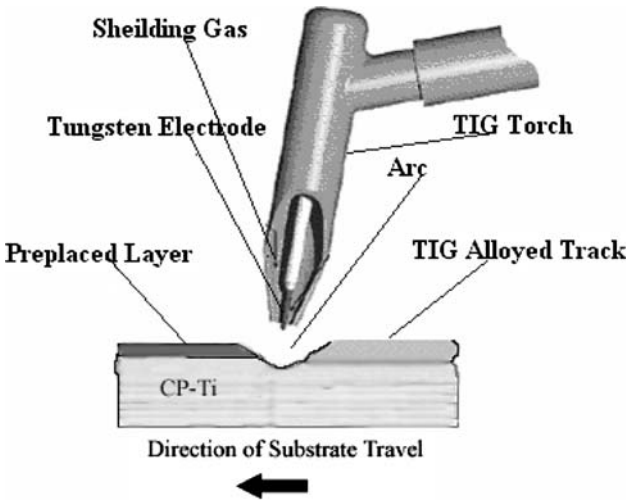

Fig. 1 Schematic of TIG surface alloying process

variable by the control device attached to the hydraulic machine. Substrate material was clamped on the x–y table. The TIG torch remained stationary while the substrate was traveled by x–y positioning table (Fig. 1).

Pure argon with the flowing rate of 15 L/min was purged into the operation chamber to prevent the surface oxidation. Surface alloying is carried out using TIG torch traversing the CP-Ti preplaced substrate to produce a series of single track without overlap (Fig. 1). The process parameters were argon gas flow rate of 6 L/min, non-consumable W electrode with 2.4 mm diameter, DC supply of about 70–130 A, voltage of 15 V, and substrate traverse speeds of 100 and 200 mm/min. The arc length was about 2 mm and the electrode polarity was chosen as DCEN. Various alloyed tracks were produced according to parameters shown in Table 1.

Specimens were prepared by cutting sections transversely to the TIG surface alloyed tracks. The specimens were then mounted in bakelite and ground down on wheels using emery papers grades from 120 up to 1,200 which were flooded with cold water. The specimens were polished on the cloth using alumina powder ranging from 7 to 0.05 μm in sequences and cleaned with water. The Kroll solution (2% HF, 10% HNO_3, and 88% H_2O) was used for etching the specimens. Finally all the specimens were washed with running water and then methanol and dried immediately.

The microstructure of the TIG surface alloyed tracks was studied using optical and scanning electron microscopes (SEM). The former was linked with an energy dispersive spectrometer (EDS). The crystal structure of the TIG surface alloyed tracks was investigated by X-ray diffraction (XRD) using CuK_α radiation generated at 40 kV and 30 mA. A microhardness tester equipped with a Vickers diamond pyramid indenter was used for microhardness

measurements along the depth of the transverse sections of the TIG alloyed tracks. A 200 g load was applied on the indenter.

The wear loss of the TIG surface alloyed tracks and untreated substrate was measured using a pin-on-disk tribometer with the test material in a conformal contact against a disk. The disk material was 40Cr13 hardened steel with a hardness value of 60 HRC. The stationary pin, 5 mm × 10 mm × 6 mm, was made from the TIG surface alloyed tracks and untreated substrate. The wear tests were performed at ambient temperature under dry conditions, normal load of 25 N, sliding speed of 0.2 ms^{-1} rpm, and a sliding distance of 400 m. The pin ran over the counter-face disk over a circular path having a diameter of 0.035 m. Prior to each test, the contacting surfaces were ground with 1,000 mesh grit SiC paper, and then they were ultrasonically cleaned in acetone, dried, and weighed to a precision of 0.1 mg. After wear test, the pin specimens have been weighed to the same precision and the weight change has been considered as wear weight-loss.

Results and discussion

Si content of the preplaced layer and heat input versus geometry and compositions of the TIG alloyed tracks

Top views of tracks No. 1 to 5 showed nearly uniform widths along their lengths and continuous build-ups (e.g., track No. 3 in Fig. 2a). However, a substantial build-up in the beginning and a distinct depression in the end of all tracks were observed. On the other hand, track No. 6, produced on the substrate with the highest Si content in the preplaced layer, was found to be discontinuous (Fig. 2b). Si is a semi-conductive element. During the production of track No. 6, arc instability was clearly observed. Thus, discontinuity of track No. 6 is attributed to the surface poor conductivity due to relatively high Si content of the preplaced powder mixture.

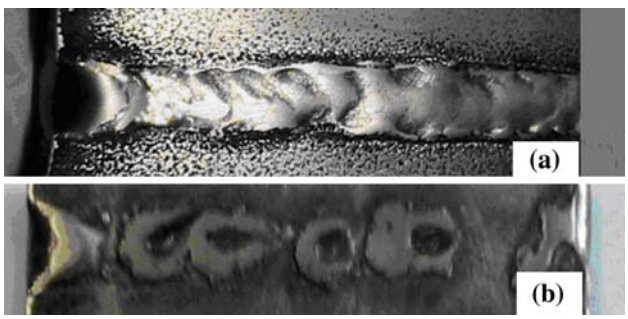

Fig. 2 Top views of the TIG surface alloyed tracks produced on CP-Ti substrate using preplaced layers with different Si amount of 30% (**a**: A continuous track No. 3.) and 50% (**b**: A discontinuous track No. 6)

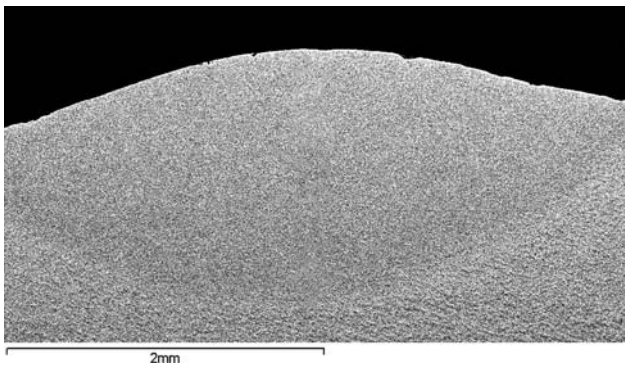

Fig. 3 Typical TIG surface alloyed tracks with conduction limited shape, electron backscattered image

Cross sections of the TIG surface alloyed tracks show melt pools with conduction limited profiles (e.g., Fig. 3).

Surface alloying using preplaced powder mixtures on CP-Ti substrate was achieved by the Si powder being mixed with the melted substrate. Chemical analyses of the TIG alloyed tracks were detected by EDS and shown in Tables 2 and 3. Homogeneity on the order of ±0.5 at.% was found based on various area analyses. In surface alloying using concentrated energy, the alloyed zone has a composition intermediate between the substrate and the introduced powder. Si content of the TIG alloyed tracks was found to be increased with the Si amount of the preplaced layers using fixed process parameters (Table 2). This is attributed to the higher Si amount of the preplaced layer being mixed with the melted substrate.

Due to high temperature of the process and the concentration gradient between the melted substrate and powder, extensive diffusion is expected, e.g., diffusion of Si in the liquid. It was suggested earlier that convective

Table 2 Si content of the TIG alloyed tracks using preplaced layer with various Si amount at the fixed process parameters

Track no.	Si in preplaced layer (at.%)	Current (A)	Substrate traverse speed (mm/min)	Si content of the alloyed tracks (at.%)
1	20	125	200	5.6
3	30	125	200	8.4
5	40	125	200	11.3

Table 3 Depth, chemical composition, and microhardness value of the TIG alloyed tracks using different heat input

Track no.	Heat input (J mm^{-1})	Depth (mm)	Si (at.%)	Ti (at.%)	Hardness (HV)
2	162	0.9	9.5	90.5	690
3	253	1.7	8.4	91.6	660
4	364	2.35	7.1	92.9	610

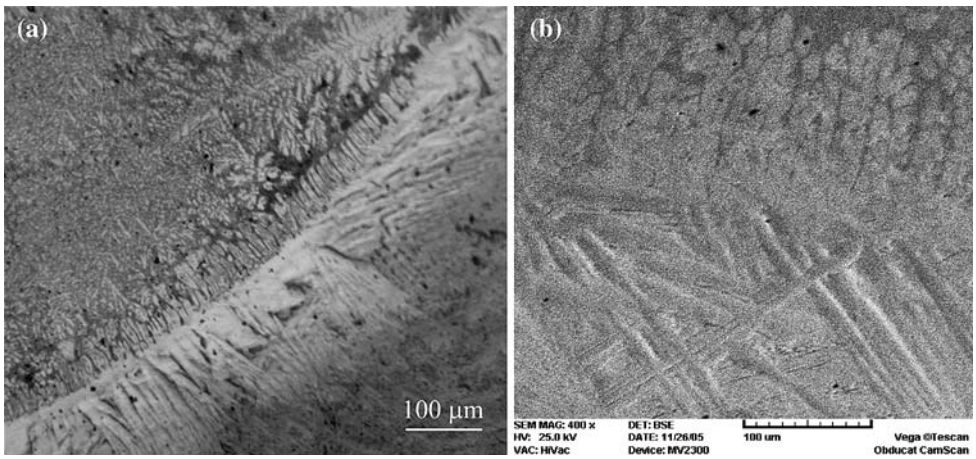

Fig. 4 Optical (**a**) and scanning electron (**b**) micrographs showing the interface of the alloyed zone/heat-affected zone

fluid flow (named Marangoni flow) phenomena which occurs due to the inhomogeneous heating of the molten pool, leading to higher temperatures in the center than at the sides can provide liquid stirring [18]. Any volume element of the surface experiences a net force parallel to the surface causing it to flow from the center to the edges of the pool. This in turn causes a return flow deep within the pool. Mazumder [19] using a two-dimensional model, considered the convection flow and heat transfer within the laser melt pool and suggested that the laser melt pool rotates approximately five times before solidification. A relatively lower solidification time and wider tracks are expected for the TIG melt pool rather than laser ones. Sufficient convective flow can distribute the alloying elements within the melt pool. Melt pool stirring transports alloying additions from the surface and distributes them throughout the melt zone.

The TIG heat input was calculated using Eq. 1 [20]:

$$\text{Heat input}(\text{J/mm}) = [0.45 \times \text{Current}(\text{A}) \times \text{Voltage}(\text{V})] / \text{Velocity}\left(\text{mm s}^{-1}\right) \quad (1)$$

The calculated values are presented in Table 3.

Si content of the TIG alloyed tracks was found to be affected by the TIG heat input. Table 3 shows different values of heat input related to tracks No. 2, 3, and 4. Higher heat input increased substrate melting progressively, giving more dilution, i.e., increased Ti and decreased Si contents of the alloyed tracks due to energy being mainly absorbed by the larger amount of the powder preplaced on the substrate. Also, increasing heat input increases the depth of the alloyed tracks (Table 3).

Microstructure

No porosity and tendency to cracking were observed. The heat-affected and alloyed zones grains were found to be epitaxially related. A network substructure was observed within the heat-affected zone grains close to the alloyed/heat-affected zones boundary. Using higher magnification, a relatively fine transformed product was observed within the heat affected zone grains (Fig. 4). The transformed phase appeared in two almost orthogonal angle variants. These are typical features of α'-Ti martensite. Such transformation products were reported by various investigators in the rapidly quenched titanium alloys [21]. Due to an increase in the temperature up to near melting point and heat sink effect of the underlining substrate, α'-Ti martensite is formed upon rapid cooling by β-Ti $\rightarrow$ α'-Ti reaction. Increasing heat input resulted in increasing volume of the heat-affected zone.

X-ray diffraction pattern of track No. 3 showed the α-Ti and ζ-Ti_5Si_3 structures to be the dominant and minor phases, respectively (Fig. 5).

The microstructures of the TIG alloyed tracks as observed on transverse sections were cellular-columnar morphologies (Fig. 4a). The cellular-dendritic structure (showing secondary arms) observed is a result of the breaking-up of the planar solidification front due to the occurrence of constitutional supercooling in the liquid ahead of the interface which depends on the ratio of G/R (Temperature Gradient/Solidification Rate) [22]; at the onset of solidification, G has its highest value and $R = 0$, the planar front forms at the

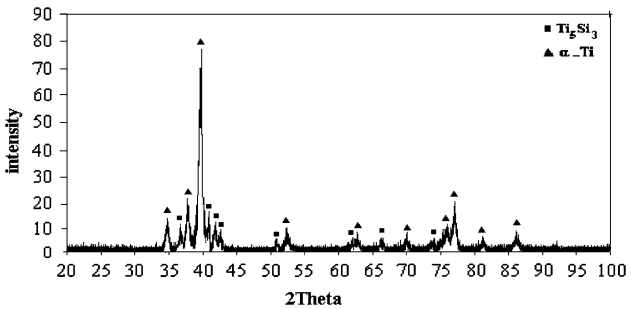

Fig. 5 X-ray diffraction pattern of track No. 3

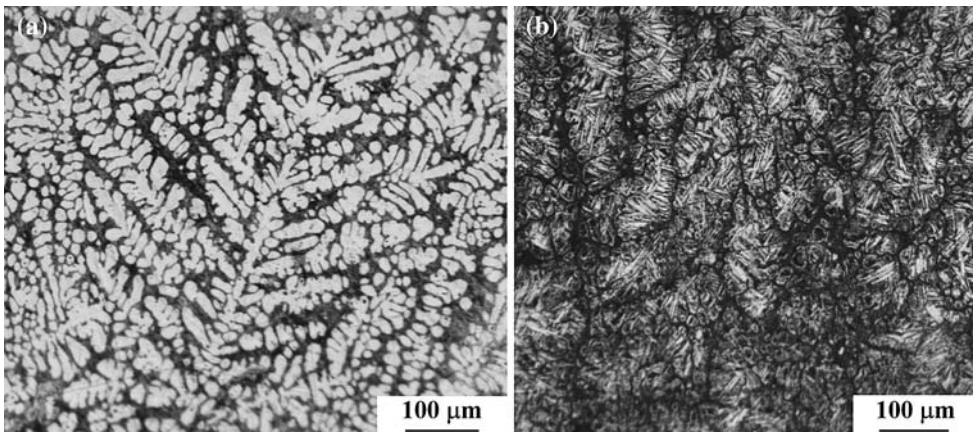

Fig. 6 Optical micrograph of surface alloyed tracks produced using different heat input of: (**a**) 162 J mm^{-1}, No. 2, and (**b**) 364 J mm^{-1}, No. 4

highest values of G/R. As solidification proceeds, the G decreases and R increases so that G/R decreases and cellular-dendritic structure forms. The higher the heat input the coarser the dendrites (Fig. 6a, b).

A martensitic-type microstructure was detected within the dendrites in track No. 4 (Fig. 6b). This is consistent with the results of Chumbley et al. [23] on the melt spun rapidly solidified Ti-6.5 at.%. Si alloy. Silicon at low levels is a β stabilizer. They detected a single-phase beta in Ti-10 and Ti-13.5Si melt spun alloys. However, the cooling rates associated with TIG surface alloying during solidification are much lower than melt spinning technique. Also, Abboud and West [24] employed laser surface alloying of titanium with silicon to produce binary Ti–Si alloyed layers. A dendritic microstructure was found in Ti–6.5Si and Ti–9Si alloyed layers. The dendrites were shown to consist of either conventional or massive martensitic structure. Dendrites with the primary spacing of 5 μm were formed which are finer than those of the TIG surface alloyed tracks ($\sim$15–50 μm); this is attributed to the higher cooling rates achieved in laser compared to TIG processing. The martensitic products documented in the Ti–Si binary alloys are hexagonal α' [21]. It is believed that finer martensitic structure is formed in the dendrite of track produced with lower heat input.

A factor favoring nucleation of the transformation which should be considered is the inhomogeneity associated with the dendritic solidification. Backscattered electron image show the interdendritic regions to be consisting of a eutectoid lamellar-type morphology (labeled A region in Fig. 7).

EDS point bulk analyses exhibited substantial differences between the dendrites (labeled B regions in Fig. 7) and interdendritic regions in the alloyed tracks (e.g., Table 4 for track No. 2). A regions show higher Si content than B regions. This scenario is consistent with the binary Ti–Si phase diagrams (Fig. 8) in which $k < 1$ partitioning coefficient values can be found for Si due to its lowering of the melting points. Thus, surface alloyed tracks have a hypo-eutectic composition including phases of primary α-Ti in dendrites and eutectic lamellas of α-Ti and Ti_5Si_3 within the interdendritic regions. Ti_5Si_3 has a phase field with compositional variations of about 5 at.% around its stoichiometric formula in the binary Ti–Si phase diagram (Fig. 8). Upon cooling, Ti_3Si is formed due to peritectoid reaction of $\beta + Ti_5Si_3 \rightarrow Ti_3Si$. However, Ti_3Si was not detected by X-ray diffraction. This is attributed to

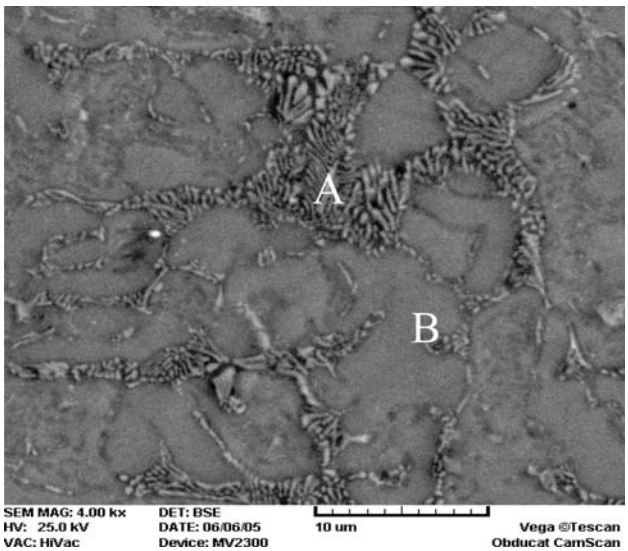

Fig. 7 Scanning electron micrograph of the surface alloyed track (No. 3)

Table 4 EDS point bulk analyses on different regions of track No. 3 (Fig. 7)

Regions	Si content (at.%)	Ti content (at.%)
A region	14.2	85.8
B region	1.3	98.7
Total regions	8.4	91.6

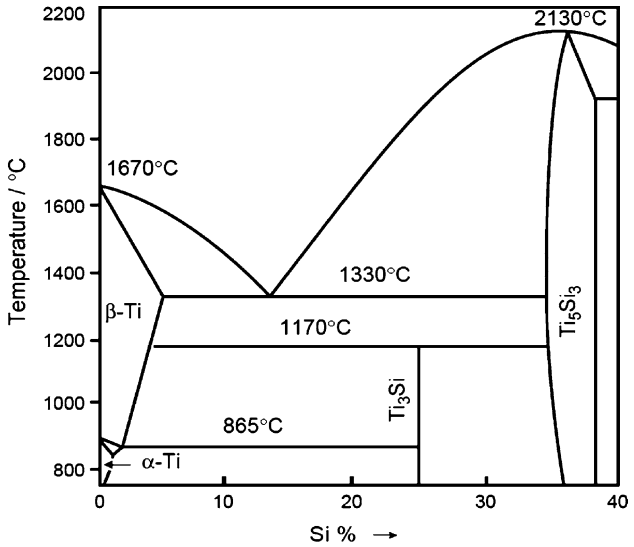

Fig. 8 Binary Ti–Si phase diagram [25]

relatively rapid cooling of the composite layers which prevented the occurance of the peritectoid reaction.

In the present investigation the Ti/Si ratio from the EDS analyses on the largest areas of silicides was higher than the 1.67 value of stoichiometric Ti_5Si_3 (Table 4); however, it should be born in mind that the silicides were finer than 500 nm (Fig. 7) so that the interaction volume associated with the EDS technique may include a region of the Ti-rich matrix thus increasing the measured rates.

Microhardness and wear resistance

The microhardness profiles along the depth of the TIG surface alloyed tracks have been shown in Fig. 9. It is apparent that TIG surface alloying with Si has significantly improved (4–5 times) the hardness; the microhardness values of the TIG surface alloyed tracks were shown to be

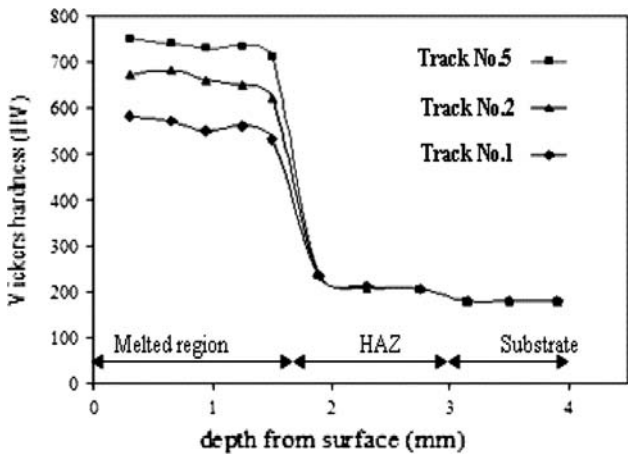

Fig. 9 Micro hardness profile of surface alloyed tracks

~4 to 5 times that of the CP-Ti substrate. It is noted that the heat-affected zone consisting of martensitic structure shows slightly higher hardness than the substrate.

The microhardness value of the TIG surface alloyed tracks showed a gradual increase with increase in the Si content. This can be attributed to the increasing volume fraction of the ζ-Ti_5Si_3 structure [11, 12, 26] and solid solution strengthening of Si in titanium. Similar trends were reported on the binary Ti–Si laser surface alloyed layers [22]. Also, the increase in microhardness with increasing silicon content is in agreement with those reported on quenched Ti–Si alloy [27]. As the heat input rate increased, the microhardness value decreased due to higher substrate dilution (Table 3) which gave lower Si content (lower volume fraction of silicides). On the other hand, the microhardness values showed to be lower than that of the Ti–Si laser surface alloyed tracks produced by Majumdar et al. [12] which are hyper eutectic and contained higher volume fraction of Ti_5Si_3 structure.

The wear weight-loss data of track No.5 (with the highest Si content) and CP-Ti substrate are presented in Fig. 10a. It is noted that the surface alloyed track has a lower weight-loss than the untreated substrate, i.e., surface alloying with silicon enhances the wear resistance of CP-Ti substrate. This behavior could be attributed to the presence of hard Ti_5Si_3 particles in the microstructure of the alloyed track with Si [11, 12]. Friction profiles for track No. 5 and CP-Ti are depicted in Fig. 10b as a function of time under the load of 25 N. It is noted that surface alloyed track has a lower coefficient of friction compared to that of the substrate.

Figures 11 and 12 show the profiles of worn surfaces of the substrate and track No. 5 after a 400 m sliding distance, respectively. CP-titanium suffers extensive typical adhesive wear dominated by plastic deformation (Fig. 11). Also, deep grooves are formed in the wear direction which is evidence of abrasive wear. On the other hand, Fig. 12 exhibits a distinct change in the surface wear mechanisms; no significant adhesive or abrasive wear has taken place in track No. 5. There is accumulation of only very fine wear debris on the worn surface.

EDS analysis of relatively large wear debris reveals high contamination content of Fe and Cr from disk to the pin surface in the case of CP-Ti substrate (Fig. 13). But no significant Fe or Cr were found in the relatively finer wear debris of track No. 5 (Fig. 14). However, XRD of this debris was not conducted due to its low volume. The EDS analyses of wear debris (Figs. 13 and 14) and the microstructural evaluation of worn surfaces (Figs. 11 and 12) substantiate the wear results presented in Fig. 10. In fact, the low friction correspond to track No. 5 may arise from partial lubrication offered by three-body wear condition involving the wear debris. Since alloyed tracks compared

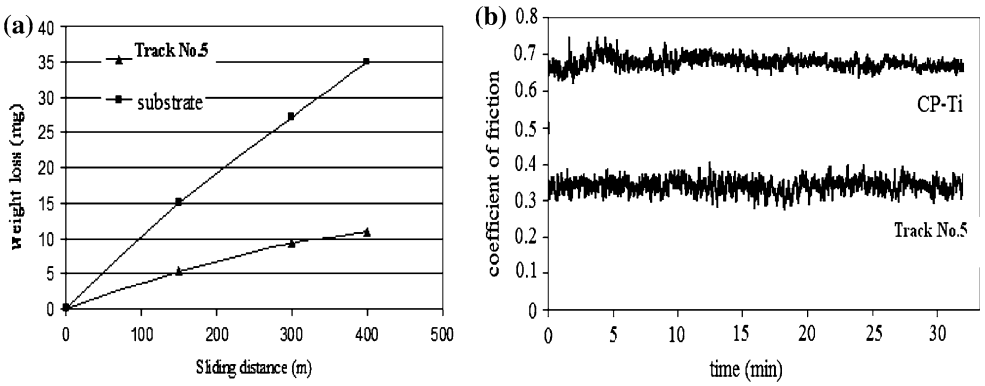

Fig. 10 Wear test results of substrate and track No. 5, (**a**) weight-loss as a function of sliding distance, (**b**) friction coefficient as a function of time

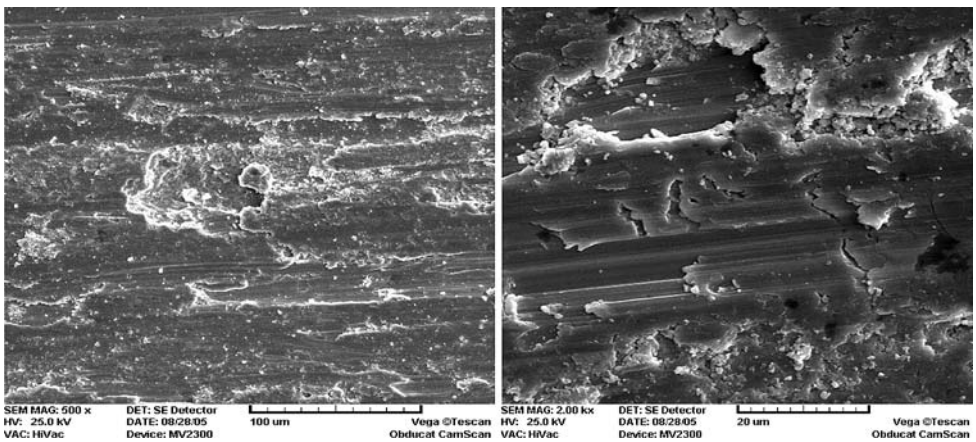

Fig. 11 SEM micrographs of the worn surface of CP-Ti substrate

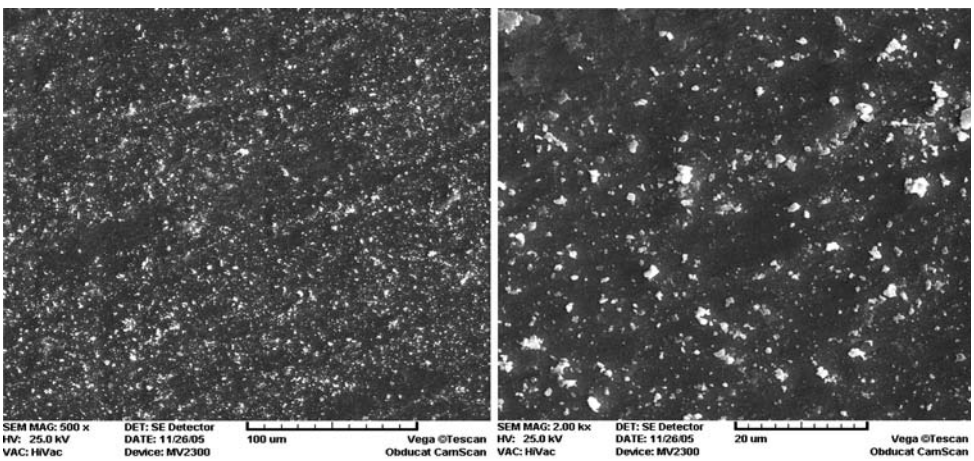

Fig. 12 SEM micrographs of the worn surface of track No. 5

to CP-Ti have hypo-eutectic two phase microstructure, therefore it can be anticipated that softer α-Ti phase in two phase microstructure of alloyed track facilitates the accumulation of wear debris of initial stage, which subsequently act as loose solid lubricant between disk and pin during the steady-state friction [12].

Conclusions

The conclusions arising from the present study could be summarized as follows:

Ti_5Si_3-based surface alloyed tracks were produced on preplaced CP-Ti substrate with Si-based paste using TIG

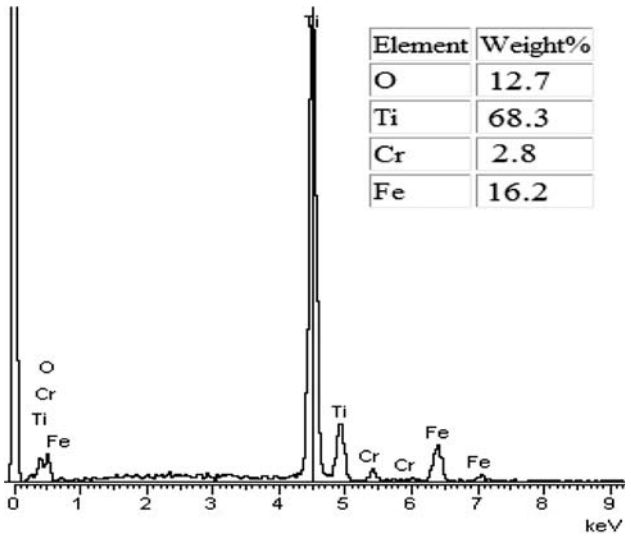

Fig. 13 EDS analysis of wear debris on worn surfaces of CP-Ti substrate

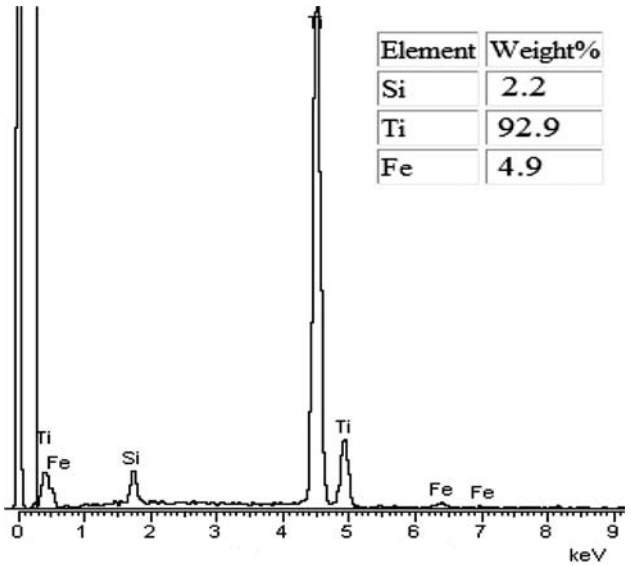

Fig. 14 EDS analysis of wear debris on worn surfaces of track No. 5

process. The microstructure of surface alloyed tracks consists of the dendrites of primary α-Ti and interdendritic regions of eutectic lamellas of Ti_5Si_3 and α′-Ti. A microhardness value of ~750 VHN was achieved in the surface alloyed tracks; this is ~4 to 5 times that of substrate material. The average microhardness value of the TIG alloyed tracks increases by increasing the Si content. The wear resistance is found to be significantly enhanced by TIG surface alloying. The superior wear behavior of the surface alloyed CP-Ti is attributed to improved microhardness values due to the presence of Ti_5Si_3 intermetallic compounds in the microstructures.

References

1. ASM handbook, vol 2-properties and selection: nonferrous alloys and special—purpose materials. ASM International (1990)
2. Handbook ASM vol 18—friction, lubrication and wear technology. ASM International (1990)
3. Budinski KG (1991) Wear 151:203. doi:10.1016/0043-1648(91)90249-T
4. Bi Q, Matthews A (2003) Surf Coat Technol 163–164:597. doi:10.1016/S0257-8972(02)00630-8
5. Pfohl C, Rie KT (1999) Surf Coat Technol 116–119:911. doi:10.1016/S0257-8972(99)00141-3
6. Lifang X, Xinxin M, Yue S (2000) Wear 246(1–2):40. doi:10.1016/S0043-1648(00)00444-0
7. Liang W, Zao XG (2001) Scr Mater 44:1049–1054. doi:10.1016/S1359-6462(01)00675-3
8. Euh K, Lee J, Lee S, Koo Y, Kim NJ (2001) Scr Mater 45:1–6. doi:10.1016/S1359-6462(01)00981-2
9. Oh J, Lee S (2004) Surf Coat Technol 179:340. doi:10.1016/S0257-8972(03)00811-9
10. Mridha S, Baker TN (1997) J Mater Process Technol 63:432
11. Tiam YS, Chen CZ, Chen LX, Huo QH (2006) Mater Lett 60:109. doi:10.1016/j.matlet.2005.07.082
12. Dutta Majumdar J, Mordike BL, Manna I (2000) Wear 242:18. doi:10.1016/S0043-1648(00)00363-X
13. Dutta Majumdar J, Weisheit A, Mordike BL, Manna I (1999) Mater Sci Eng A 266:123. doi:10.1016/S0921-5093(99)00045-3
14. Wenbin D, Haiyan J, Xiaoqin Z, Dehui L, Shoushan Y (2007) J Alloy Compd 429:233. doi:10.1016/j.jallcom.2006.03.083
15. Baytoz S, Uttran M, Mustafa M (2005) Appl Surf Sci 252:1313. doi:10.1016/j.apsusc.2005.02.088
16. Mridha S (2005) J Mater Process Technol 168:471–477. doi:10.1016/j.jmatprotec.2005.02.247
17. Mridha S, Ong HS, Poh LS, Cheang P (2001) J Mater Process Technol 113:516. doi:10.1016/S0924-0136(01)00609-4
18. Anthony TR, Cline HE (1977) J Appl Phys 48(9):3888. doi:10.1063/1.324260
19. Chade T, Mazumder J (1983) Metall Trans 14B:181
20. Easterling KE (1992) Introduction to the physical metallurgy welding. Butterworth-Heinemann, London
21. Flower HM, Swann PR, West DRF (1972) J Mater Sci 7:929. doi:10.1007/BF00550440
22. Kurz W, Fisher DJ (1984) Fundamentals of solidification. Trans Tech Pub., Netherlands, p 71
23. Chumbley LS, Ohles MA, Fraser HL (1986) In: Froes FH (ed) Titanium rapid solidification technology. TMS-AIME, Warrendale, PA, p 211
24. Abboud JH, West DRF (1991) Surf Eng 7(2):159
25. Massalski TB, Okamoto H, Subramanian PR, Pkacparzak L (1990) Binary alloy phase diagram. ASM International, Material Park, OH
26. Fasasi AY, Roy SK, Galerie A, Pons M, Caillet M (1992) Mater Lett 13:204
27. Bumps ES, Kessler HD, Hansen M (1953) Trans ASM 45:1008